Supporting Information-Table of Contents

Novel hyperoxidation resistance motifs in 2-Cys peroxiredoxins
Bolduc et al.

Fig. 1. Kinetic analysis of hPrx1-3 reveals 3-25-fold differences in hyperoxidation sensitivity.

Fig. 2. Superposition of human Prx2 and human Prx1 structures.

Fig. 3. Large-scale sequence alignment reveals putative resistance-conferring motifs, Motif A and Motif B.

Fig. 4. Assessment of all protein constructs by circular dichroism.

Fig. 5. MS/MS spectra of AhpC C46-containing peptide in representative oxidized states: (top) carbamidomethylated peptide resulting from blocking of reduced thiol with iodoacetamide, (middle) oxidized -SO_2H state, and (bottom) oxidized -SO_3H state.

Table 1. Data collection and refinement statistics.

Table 2. Proteins used for WebLogo analysis and the amino acids present at motif A and B.

Table 3. CD, melting temperature and HRP analysis for wild type proteins and variants.

Table 4. Theoretical and experimental mass values for the different oxidation states of Prx1 and Prx2 variants.

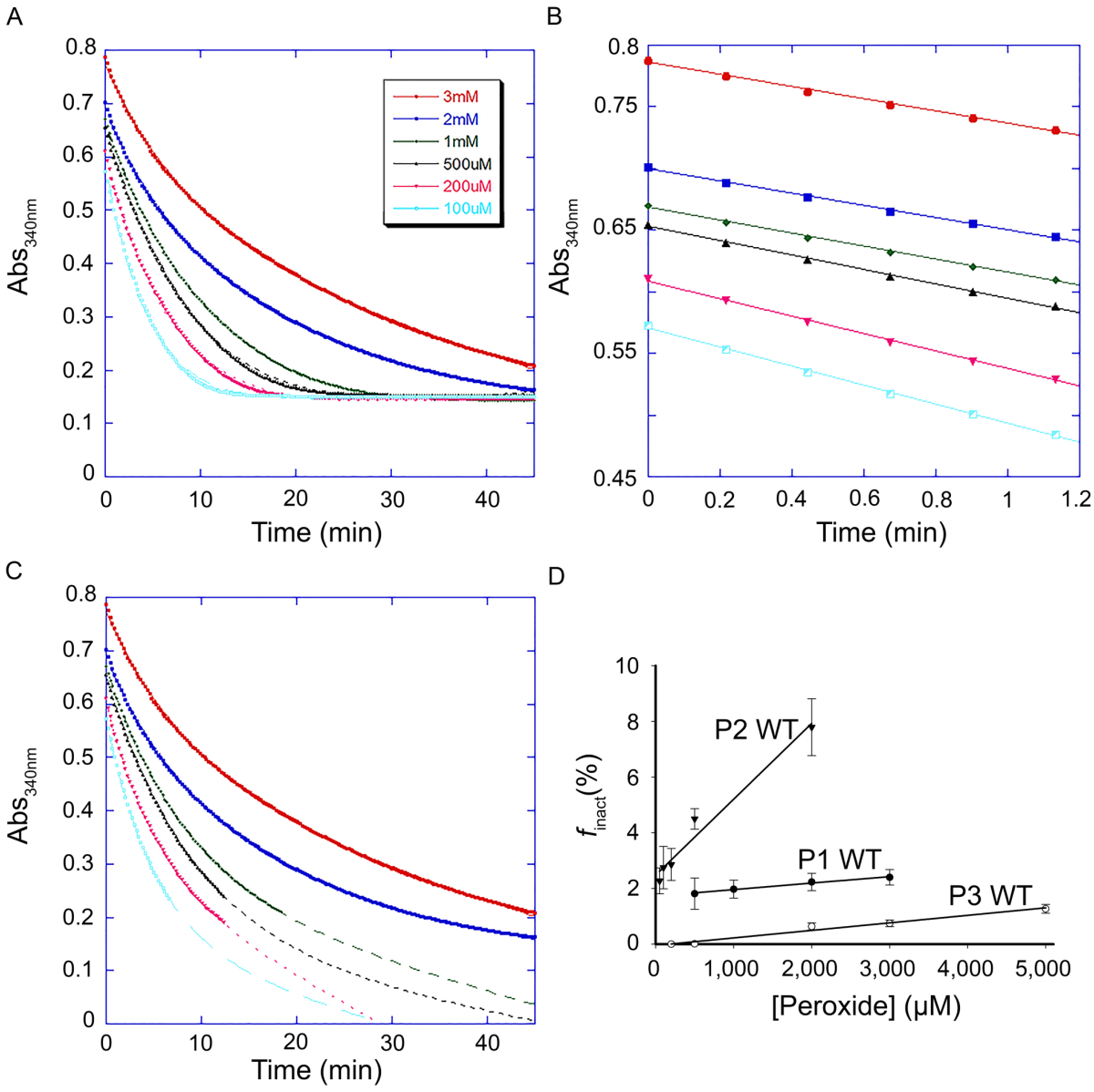

Figure 1. Kinetic analysis of hPrx1-3 reveals 3-25-fold differences in hyperoxidation sensitivity. *A*, Representative plot of the loss of Prx1 peroxidase activity. Activity was determined by monitoring the decrease in absorbance over time at 340 nm, from the consumption of NADPH by the *E. coli* Trx-TrxR-NADPH system. The reaction mixture was optimized for each Prx variant tested in this study and contained the following components and final concentrations: 0.25-2.5 μM Prx, 5-10 μM Trx, 0.2-0.5 μM TrxR, 150 μM NADPH. H_2O_2 was added to a final concentration of 50-5000 μM to start the reaction. The reactions were performed at 25°C. The curvature in the plot at later time points illustrates the Prx inactivation process, especially with increasing peroxide concentration. All Prx proteins and peroxide concentrations used within this study were analyzed on 3 or more separate days with fresh aliquots of each protein (Prx, Trx and TrxR) and H_2O_2. Each day included 3-4 technical duplicates. *B*, Slope of the initial linear portion used to approximate the $k_{SS}K_{LU}$ rate. The slope of the initial linear portion was determined using the readings from the first five time points. The peroxide concentrations used are indicated in the legend within panel *A*. Please see the methods section for a description of the rationale for this procedure and the equations used. *C*,

Exponential decay rate used to approximate the rate of inactivation, k_{SO2H}. The raw data was fit to equation 4. *D*, Plot of fraction inactivated, f_{inact}, versus peroxide concentration. The exponential rate was divided by the initial linear rate to give the f_{inact} at each peroxide concentration. The reciprocal of the slope of this plot divided by 100 is the $C_{hyp1\%}$ value. All data were used for f_{inact} and $C_{hyp1\%}$ calculations. The $C_{hyp1\%}$ values determined for hPrx1, hPrx2, and hPrx3 were as follows: 50 μM, 5 μM, and 127 μM, respectively.

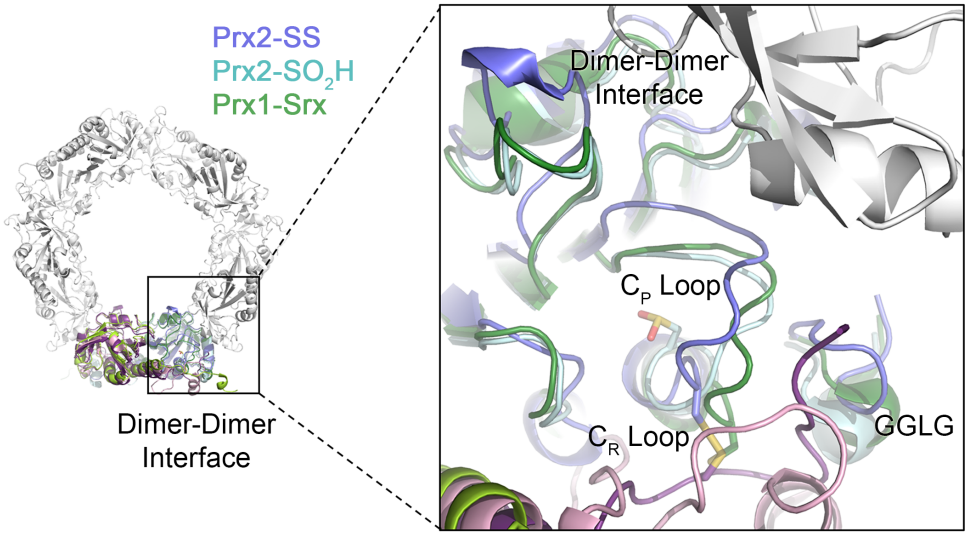

Figure 2. Superposition of human Prx2 and human Prx1 structures. Prx2-S_PS_R and Prx2-S_PO_2H are colored the same as in Fig. 2. The Prx1 (locally unfolded) molecule from the Prx1-Srx complex is shown in green; Srx has been omitted for clarity (PDB code 2RII) (22). The adjacent dimers of the toroid are shown in white. A close-up view shows numerous positional changes of the loops at the dimer interface, the GGLG motif, and the loops that contain the Cys-S_P and Cys-S_R residues (C_P loop and C_R loop). The hyperoxidized Cys51 of Prx2 is in the center of the view for reference.

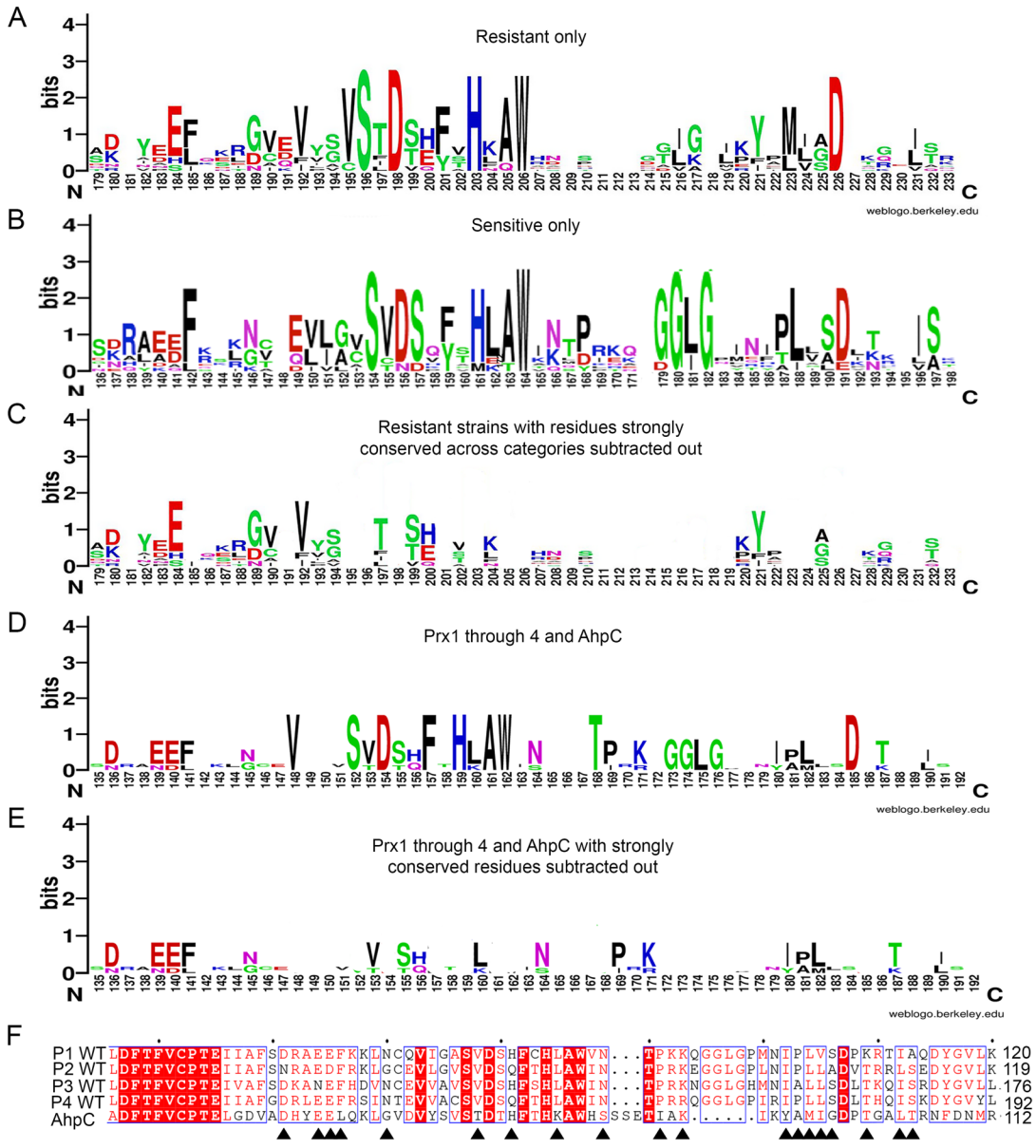

Figure 3. Large-scale sequence alignment reveals putative resistance-conferring motifs, Motif A and Motif B. *A*, WebLogo plot for the regions of interest for a grouping of robust Prxs. Information for the proteins analyzed is given in supplemental Table 2. *B*, WebLogo plot for the regions of interest for a grouping of sensitive Prxs. *C*, Subtractive alignment where residues that were strongly conserved in sensitive and robust Prxs were removed from the plot. We assumed that these residues did not play a role in modulating hyperoxidation sensitivity. *D*, WebLogo plot for human Prxs 1 through 4 and AhpC. *E*, Subtractive alignment where the residues that were strongly conserved amongst the hPrx1-4 and AhpC were removed from the plot, in the same manner as (*C*). This process left residue positions that had ~50% occurrence between two different residues, which we hypothesized was the way to distinguish between two different populations: robust and sensitive. *F*, Residues selected for comparison to the Prx2-S_PS_R structure and Prx1/2 alignments (also shown in Fig. 2 and Fig. 3 in the main text). Residue positions (solid triangles) that were split 50/50 and represented significant changes in character (i.e., charge, hydrophobicity, and size) were focused on for motif identification.

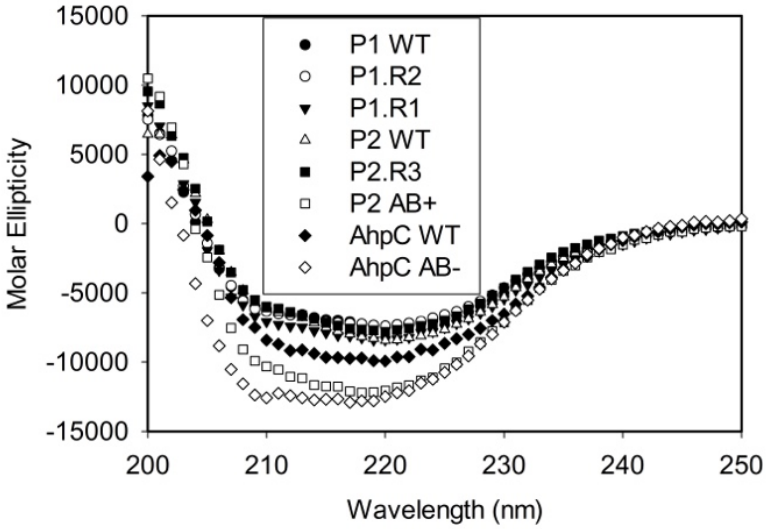

Figure 4. Assessment of all protein constructs by circular dichroism. Samples were pre-reduced with 10mM DTT for a minimum of 30 minutes and then desalted. Afterwards, proteins were diluted to approximately 20 µM in 7 mM phosphate buffer saline (PBS). CD spectra were scanned over wavelengths from 250-180 nm with three technical repeats and averaged. Molar ellipticities and helical content were calculated from the averaged data. CD spectra were repeated 2-3 times on separate days with three technical repeats each day. See supplemental Table 3 for melting temperatures and helical content analysis.

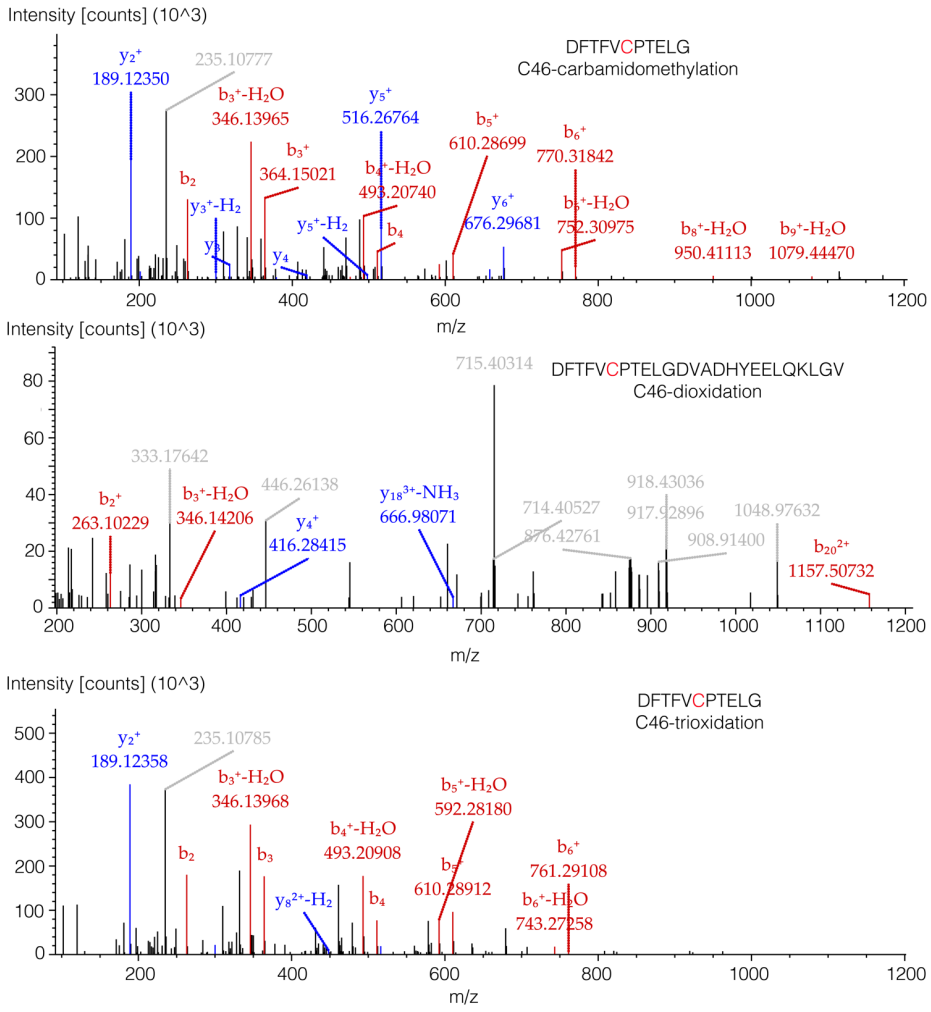

	AhpC.WT		AhpC.AB⁻			
	-SO_2H		-SO_2H		-SO_3H	
	-H_2O_2	+H_2O_2	-H_2O_2	+H_2O_2	-H_2O_2	+H_2O_2
Ratio of Oxidized Species Relative to Untreated Controls	1.0	1.2	1.0	1.0	1.0	11.0

Figure 5. MS/MS spectra of AhpC C46-containing peptide in representative oxidized states. (top) carbamidomethylated peptide resulting from blocking of reduced thiol with iodoacetamide, (middle) oxidized -SO_2H state, and (bottom) oxidized -SO_3H state. The Table represents a summary of the ratios of -SO_2H and -SO_3H states in H_2O_2 treated samples relative to the untreated controls. The ratios were calculated using the peak area of the respective extracted ion chromatogram in each sample using Skyline. The bar graph representation of the data is shown in Fig. 4*F* of the main text.

Table 1. Data collection and refinement statistics.

	Prx2 SS
Data collection	
Space group	$P2_1$
Cell dimensions	
a, *b*, *c* (Å)	50.0, 198.8, 116.5
α, β, γ (°)	90.0, 96.3, 90.0
Resolution (Å)	44.5−2.2 (2.23−2.15)*
R_{merge} (%)	6.6 (73.7)
$I / \sigma I$	19.1 (2.8)
Completeness (%)	99.6 (97.9)
Redundancy	6.6 (6.6)
$CC_{1/2}$	0.85
Wilson B ($Å^2$)	49.7
Refinement	
Resolution (Å)	44.5−2.15
No. reflections	122,121
R_{work} / R_{free} (%)	20.7/25.7
No. atoms	
Protein	13,141
Ligand/ion	4
Water	95
B-factors	
Protein	70.8
Zn^{2+}	108.0
Water	51.3
R.m.s. deviations	
Bond lengths (Å)	0.016
Bond angles (°)	1.33
PDB code	5IJT

*Values in parentheses are for highest-resolution shell. Data is from one crystal.

Table 2. Proteins used for WebLogo analysis and the amino acids present at motif A and B.

Protein	UniProt Entry #	Residues in Motif A	Residues in Motif B
Robust			
***Salmonella typhimurium* AhpC**	P0A251	DGHG	TT
***Schistosoma mansoni* TPx1**	O97161	DNQA	KS
***Schistosoma mansoni* Prx3**	G4LXH7	DGHA	QT
***Salmonella typhimurium* TsaA**	A0A0K6PMJ5	KGEA	KQ
***Amphibacillus xylanus* AhpC**	O87200	KGHG	SS
***Mycobacterium tuberculosis* AhpC**	A0A0K0YAZ0	KDES	KS
***Treponeme pallidum* AhpC**	O83522	RGES	AA
***Vibrio vulnificus* AhpC (185)**	A0A087IM46	DGHG	TT
***Vibrio vulnificus* AhpD (177)**	A0A087IH97	ND--	--
Sensitive			
***Homo sapiens* Prx1**	Q06830	DNHS	KA
***Homo sapiens* Prx2**	P32119	NGQA	TS
***Homo sapiens* Prx3**	P30048	DNHS	TS
***Homo sapiens* Prx4**	Q13162	DNQS	TS
***Oryza sativa* 2-Cys Prx**	Q9FR35	DNVS	TS
***Clostridium pasteurianum* 2-Cys Prx**	P23161	KKQS	TS
***Plasmodium falciparum* TPx1**	Q9N699	KNKS	TS
***Schistosoma mansoni* TPx2**	Q9Y0D3	EGVS	NS
***Plasmodium falciparum* TPx2**	Q9BKL4	KNVS	NS
***Synechococcus sp.*2-Cys Prx**	A0A0H5PQL7	DNES	KS
Variants in this study			
P1.R1	-	DGHS	KA
P1.R2	-	DNQS	KA
P2.R3	-	NGQS	KA
P2.AB^{+}	-	DNHS	TS
AhpC.AB^{-}	-	NNQA	KA

Table 3. CD, melting temperature and peroxidase activity analysis for wild type proteins and variants.

Variant	Helical Content (%)	T_M (°C)	k_{SOH} (M^{-1} s^{-1}) x 10^6
P1.WT	21 ± 1	57.3	5 ± 1
P1.R1	24 ± 5	61.0	22 ± 4
P1.R2	21 ± 1	63.1	8 ± 1
P2.WT	23 ± 2	57.9	6 ± 1
$P2.AB^+$	34 ± 1	67.8	18 ± 2
P2.R3	22 ± 1	49.6	18 ± 5
AhpC.WT	25 ± 2	42.8	23 ± 6
$AhpC.AB^-$	34 ± 2	53.2	6 ± 1

Table 4. Theoretical and experimental mass values for the different oxidation states of Prx1 and Prx2 variants.

	Mass Values $[M+H]^{+1}$ (amu)					
Oxidation State	**Observed**	**Theoretical**	**Observed**	**Theoretical**	**Observed**	**Theoretical**
	P1.WT		**P1.R1**		**P1.R2**	
SH	21979.9	21980.3	21924.3	21924.2	21965.9	21966.2
SOH	21996	21996.3	21940.6	21940.2	21982.3	21982.2
SO_2H	22012	22012.3	21957.5	21956.2	21997.7	21998.2
SO_3H	22028.2	22028.3	-	21972.2	22014.1	22014.2
	P2.WT		**P2.AB^+**		**P2.R3**	
SH	21761.7	21761.7	21844.6	21844.6	21716.7	21716.8
SOH	21779.7	21777.7	21861.5	21860.6	21734.4	21732.8
SO_2H	21793.7	21793.7	21877.3	21876.6	21748.7	21748.8
SO_3H	21811.3	21809.7	21896.3	21892.6	21766.3	21764.8